17th AIAA International Space Planes and Hypersonic Systems and Technologies Conference
11 - 14 April 2011, San Francisco, California

AIAA 2011-2373

Investigation of Structure for the Hypersonic Transport System SpaceLiner

A. Kopp[1], A. van Foreest[2] and M. Sippel[3]
German Aerospace Center (DLR), Space Launcher Systems Analysis (SART), Bremen, 28359, Germany

M. Dalenbring[4] and R. Jarlas[5]
Swedish Defence Research Agency (FOI), Aeronautics and Systems Integration, Stockholm, SE-164 90, Sweden

The Space Launcher Systems Analysis group (SART) of the German Aerospace Center (DLR) has been working for several years on the SpaceLiner, a novel concept for hypersonic intercontinental travel. The SpaceLiner is currently also under investigation in the EU-funded FAST20XX study, with contributions from several partners. The present paper focuses on the structural preliminary design and summarizes the works performed so far on structural and TPS layout. A large number of load cases have been defined and will be described. Special attention will be paid to the detailed wing design and corresponding static- and dynamic- structural analysis. Also, integration of wing and fuselage and the resulting structural-dynamic vehicle characteristics will be illuminated. A discussion concerning the preliminary TPS concept will follow. Finally, a brief outlook on some future activities will be presented.

Nomenclature

C.O.G	=	Center of Gravity
E	=	Young's modulus
G	=	Shear modulus
H	=	altitude
Ma	=	Mach number
n_x	=	axial acceleration
n_z	=	normal acceleration
q	=	dynamic pressure
T_b	=	back-structure temperature
TPS	=	Thermal Protection System
v	=	velocity
α	=	angle of attack
ν	=	Poisson's ratio
ρ	=	density
σ_{all}	=	allowable stress

[1] Research Scientist, Space Launcher Systems Analysis, DLR, Member of AIAA.
[2] Research Scientist, Space Launcher Systems Analysis, DLR, Member of AIAA.
[3] Head, Space Launcher Systems Analysis, DLR.
[4] Senior Scientist, Aeronautics and Systems Integration, FOI.
[5] Senior Scientist, Aeronautics and Systems Integration, FOI.

I. Introduction

SINCE 2005, the Space Launcher Systems Analysis group (SART) of the German Aerospace Center DLR has been working on a novel vehicle concept for long range hypersonic passenger transport. The "SpaceLiner" is a large, rocket propelled vehicle that is launched vertically with launch and ascent being assisted by a reusable booster. Both, the hypersonic passenger stage and the booster utilize liquid propellants. Several papers concerning the general vehicle layout, mission, trajectory and logistic challenges have been published in the recent years.[1,2] The SpaceLiner is also one of two vehicle concepts investigated by the partners within the current European Union space tourism research project FAST20XX. Fig. 1 shows an artist's impression of the SpaceLiner system at booster separation.

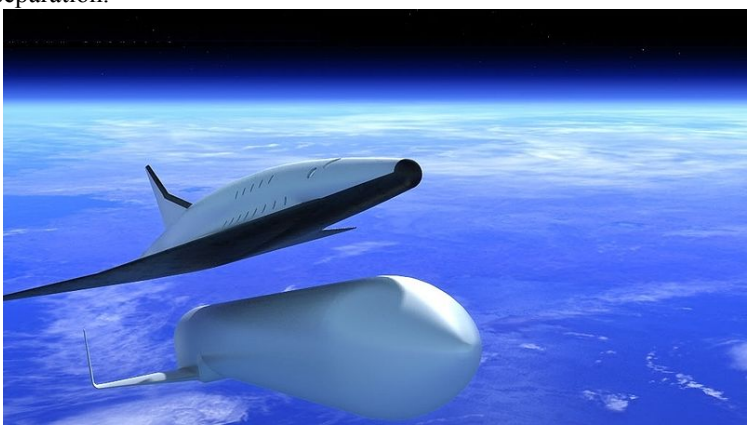

Figure 1. Artist's impression of the SpaceLiner2 at booster separation.

In contrast to other hypersonic vehicle concepts the SpaceLiner does not incorporate radically new or unproven technologies. Instead, rather conventional rocket propulsion systems and vertical ascent trajectories are used. Thus, the development of such a vehicle is more a political and financial question, and to a lesser extend a technological one. Nevertheless the SpaceLiner concept contains several technical and logistical challenges, such as active cooling technologies, passenger accommodation and safety together with the provision for suitable launch and landing sites.

The final objective of the SpaceLiner development is to dramatically reduce intercontinental travel times compared to today's subsonic passenger aircraft flights by travelling at hypersonic velocities. For example, a trip from Europe to Australia, which is the current reference mission, will last only 90 minutes. Also other intercontinental routes such as New York to Australia have been considered. However, the advantage in total travel time is reduced for shorter flight distances since the flight preparation times for the passengers are higher than for a conventional flight.

Building and operating a comparatively large number of SpaceLiner vehicles will also have a significant impact on the space launcher industry. Even if only a very small portion of the long range intercontinental passenger transport will be covered by the SpaceLiner, the resulting annual launch rates would multiply compared to the present situation and greatly reduce operation costs. Production rates for reusable launch vehicles and their engines would dramatically increase, resulting in lower production costs.

A more detailed discussion of the system aspects for the SpaceLiner will be published in Ref. 3.

A. General Description of the SpaceLiner Concept

The SpaceLiner is a two stage, vertical launch system with a LOX/LH2 fueled, reusable booster and a passenger stage, also called "orbiter", which utilizes the same propellants as the booster. Both stages are fully reusable and equipped with wings for gliding return flight. After launch the system climbs to an altitude of about 73 km, where the booster separation takes place. The booster will immediately return to the launch base. The orbiter will accelerate further to an altitude of 80 km and a velocity of 6.7 km/s by its own propulsion system. After main engine cut off (MECO) the gliding flight phase begins. Initially the SpaceLiner was planned to utilize a so called skipping trajectory, which was thought to maximize the range. However, it was also found that this kind of trajectory leads to comparatively high heat loads, increasing the mass for the thermal protection systems. Recent trajectory optimizations have yielded a smooth trajectory wich avoids any skipping, while greatly improving passenger comfort and reducing the heat loads[3]. The small increase of propellant mass for the new trajectory profile is more than balanced by a lower TPS mass. In addition to the trajectory improvement, the vehicle shape has also changed. The design which is currently under development and will be discussed in this paper is the SpaceLiner7. Fig. 2 shows a potential design option for the SpaceLiner7, while Fig. 3 illustrates the earlier SpaceLiner4 design. The wing shape has been changed from the original double delta wing to a highly swept single delta wing to improve hypersonic cruise characteristics. More information on the evolution of the SpaceLiner design including the SpaceLiner5 and SpaceLiner6 variants can be found in Ref. 3.

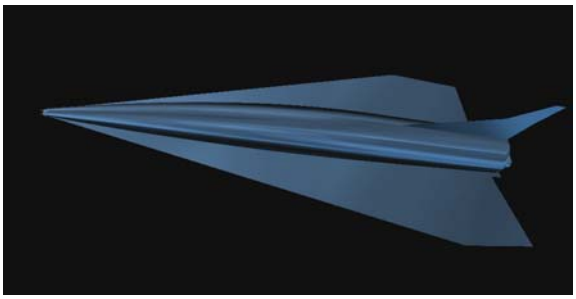

Figure 2. Potential design option of SpaceLiner7 passenger stage.

The general layout of the SpaceLiner7 is however far from being finalized. Up to now the outer shape has been mainly determined by propellant and passenger accommodation issues as well as aerodynamics and aerothermodynamics. Now, structural considerations become more and more important for the vehicle layout.

The current design is planned for a payload of 50 passengers. The passengers and crew are accommodated in a separate rescue capsule, which is partly integrated in the primary structure of the passenger stage and can be separated in case of an emergency at any point during the mission. A preliminary design of the rescue capsule has already been created. Fig. 4 shows a corresponding CAD drawing.

Structural and TPS preliminary layouts for the SpaceLiner passenger stage are subject to ongoing works at DLR-SART and its partners in the FAST20XX study. The present paper sums up the current status of these activities and describes the initial structural layout. The structural design for the booster has not been investigated so far and will not be discussed here.

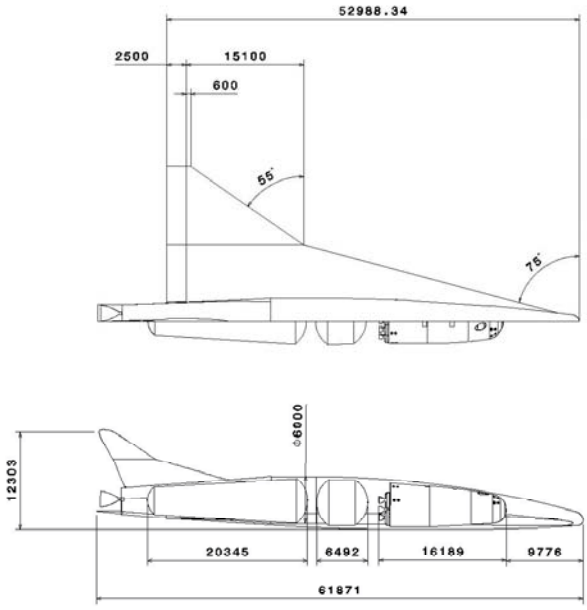

Figure 3. SpaceLiner4 latest layout of the passenger stage.

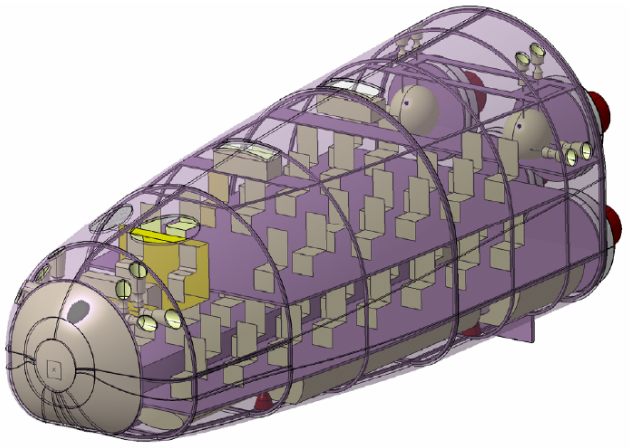

Figure 4. SpaceLiner rescue capsule.

II. Definition of Load Cases

The structural design of a complex flight vehicle system requires consideration of a large number of load cases. Some load cases will only be relevant for sizing of components such as wings, fins or even their subcomponents. Other load cases are design drivers for the structural layout of the complete vehicle. A careful investigation has to be carried out to identify all critical load cases. As a first step it is useful to perform a "brainstorming" to generate and collect all cases that may have an impact on structural sizing. Consequent detailed analysis then allows for the definition of those load cases which are deemed to be relevant. Early considerations yielded in a large number of potential load cases for the SpaceLiner system. Thus, a classification system with the four categories "system", "booster", "orbiter" and "rescue capsule" has been defined. In this context the category "system" comprises load cases that occur while booster and orbiter are still connected. For each category the load cases have been further grouped according to the flight phase during which they may occur. Since the focus of this paper is the structural layout of the orbiter, only the load cases relevant for the orbiter and the complete system will be discussed here. Table 1 lists the potential load cases for the complete system as collected so far. Table 2 shows the corresponding load cases for the separated passenger stage. Some positions in both tables are still unspecific such as "aeroelastic" and need to be defined in more detail. As may be observed several load cases can be found in both tables, since

these cases may lead to different load conditions for the unseparated and the separated stage. For instance the maximum axial acceleration of the complete system prior to stage separation generates other loads for the passenger stage than the maximum acceleration of the stage after separation. In the first case the passenger stage is connected to the booster and is partially pulled by the latter, while in the second case the passenger stage is running on its own rear-mounted engines only, inducing compressive loads.

Table 1. Load cases for the complete system.

Complete system	
ID	**Description**
Ground handling	
S-1-01	Integration (including component transport)
S-1-02	Erecting in vertical position
S-1-03	Transport – wind / gust (on carrier vehicle)
S-1-04	Transport – vibrations
S-1-05	Launch pad (empty tank, unpressurized)
S-1-06	Launch pad (full tank, unpressurized)
S-1-07	Launch pad (full tank, pressurized)
Lift-off – vertical flight	
S-2-01	100% thrust hold case
S-2-02	Dynamic thrust overshoot
S-2-03	Acoustic effects due to SPL
S-2-04	Vibrations
Powered ascent	
S-3-01	Maximum n_x acceleration
S-3-02	Maximum dynamic pressure q
S-3-03	Maximum $q \cdot \alpha$ due to wind / gust
S-3-04	Maximum acceleration imbalance booster - orbiter
S-3-05	Aerodynamic interferences booster - orbiter
Non-nominal	
S-6-01	Mission abort at maximum n_x acceleration
S-6-02	Mission abort at maximum dynamic pressure q
S-6-03	Mission abort at maximum $q \cdot \alpha$
S-6-04	Mission abort at maximum acceleration imbalance
S-6-05	Engine failure
S-6-06	Random vibration due to POGO
S-6-07	FO impact on critical stage attachment parts
S-6-08	TVC actuator failures

Table 2. Load cases for the passenger stage.

Passenger stage / "Orbiter"	
ID	**Description**
Ground handling	
O-1-01	Ground transportation
O-1-02	Maintenance
Ascent	
O-3-01	Separation
O-3-02	Maximum n_x acceleration (after stage separation)
Cruise / re-entry	
O-4-01	Maximum thermal loads
O-4-02	Maximum flap and rudder deflection
O-4-03	Maximum normal n_z acceleration (2.5 g)
O-4-04	Combination of thermal and mechanical loads
O-4-05	Maximum horizontal stabilizer load
O-4-06	Aeroelastic
Landing	
O-5-01	Wind / gust
O-5-02	Landing shock (for main and nose gear separately)
O-5-03	Braking
Non-nominal	
O-6-01	Maximum normal n_z load (non nominal)
O-6-02	Abort scenario (tbd g)
O-6-03	Crash landing w/o landing gear
O-6-04	Crash landing with one gear
O-6-05	Landing on rough runway
O-6-06	Wing tip strike
O-6-07	Tail strike
O-6-08	Lightning strike
O-6-09	Critical FO impact (e.g. bird strike)
O-6-10	Combination of thermal and mechanical loads
O-6-11	LOX tank internal sloshing
O-6-12	LH2 tank internal sloshing

A. Discussion of the Load Cases

Ground integration and transportation may generate several load cases for the passenger stage when connected to the booster as well as for the "stand alone" conditions. The load cases collected in this mode of operation are similar to classical rocket launcher loads analysis. On the launch pad and during transport on a carrier vehicle in a vertical position the launcher is exposed to wind and gust loads. Both, transport and launch pad have been listed separately since it is not clear if the mounting conditions will be identical. Further load cases will be generated when considering the propellant tanks in unpressurized and pressurized, unfilled and filled condition.

Lift off and ascent phases again generate load cases similar to those for typical rocket launchers. A special load case to consider is the case generated by aerodynamic interferences between booster and orbiter. Currently, it is not clear if the complex flow field between booster and orbiter will cause relevant structural-dynamic effects or even local thermo-structural problems due to compression shock impingement.

The cruise/re-entry load cases are only relevant for the separated stage and include thermo-structural loads, rudder/flap deflections, stabilizer loads and maximum normal accelerations. To fulfill civil aviation requirements a maximum normal acceleration of 2.5 g is assumed.[4]

Landing load cases are similar to those for general aviation. However civil aviation requirements demand consideration of a number of additional load cases that have not been taken into account here.[4]

Finally, a large number of non-nominal load cases have been identified for both-, the separated and unseparated conditions. This includes an abort scenario, where the passenger stage performs an emergency separation from the booster and returns to a suitable runway. The remaining LH2 and possibly also the LOX may be dumped to assure safe landing and prevent fatal explosions in the case of a crash landing. Such an abort scenario may occur during every phase of the ascent. Recent calculations indicated that the passenger stage will be able to perform abort maneuvers within the 2.5 g normal acceleration limit.[3] These calculations have also taken vehicle trimming into

account. Further load cases may originate from non-nominal landing conditions such as landing on rough runways, wing tip or tail strikes, and crash landings with no gears or only one. Of course, also lightning strikes and critical foreign object impacts have to be accounted for. Other, more typical rocket launcher type load conditions have been listed including POGO vibrations and propellant sloshing.

B. Selection of Load Cases for Preliminary Structural Sizing

In an early development phase it is of course not possible to take into account all load conditions that have been listed in Table 1 and Table 2. Thus, it is necessary to define a number of load cases that are thought to be design drivers and consider the possible impact of further load cases by reasonable margins. In fact it is a typical experience in flight vehicle structural design that the system mass increases when the number of considered load cases is increased.

It has been decided to follow an approach where the typical load cases used for rocket launcher or aircraft preliminary design are considered first. They will then be supplemented step by step by cases that go more into detail. However, several load cases require deeper analysis such as crash landings and other damage tolerance issues. Their consideration may be a subject for the next phase of structural analysis.

In the following section the load cases selected so far for the initial wing analyses will be discussed in more detail.

III. Preliminary Structural Design of the Passenger Stage

The structural analysis performed so far placed strong emphasis on the wing design, while the fuselage structure investigations started recently. Thus, this section focuses on the design of the wing structure. For the fuselage only a rough model has been generated up to now to allow for structural-dynamic analyses.

The wing structure analysis was done in three steps. Initially, the arrangement of the structural members has been fixed. For this task an investigation on the required main gear and flap dimensions and wing integration had to be performed. In the second step a static optimization of the wing structure has been conducted. The third step finally incorporated a structural-dynamic analysis and corresponding adaption of the structure.

The less detailed fuselage model and the wing have been connected and dynamic investigations have been performed for the total passenger stage structure.

A. Wing Structure Design

For the initial wing layout it has been decided to adopt a more detailed approach compared to the typical simplified analysis procedures in the early design phase. This includes main gear integration and rudder/flap loads introduction. The wing plan form has been fixed in previous aerodynamic investigations. NACA-66 has been selected as the wing profile. The main dimensions are described in Fig. 5.

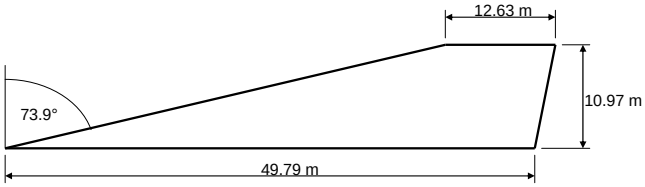

Figure 5. Basic geometry of the wing.

1. Main Gear Dimensions and Accommodation

Due to the vertical take off the SpaceLiner passenger stage requires only a relatively light weight landing gear. Thus, a simple "drop down" approach without complex mechanisms and actuators for gear deployment would be possible. Therefore it is beneficial to have a non-folding gear which however requires a landing gear bay at least as long as the gear. A trade off has been done to define the main gear position and length. To maximize the load carried by the main gear and minimize the nose gear load it is favorable to place the main gear as far forward as possible, which on the other hand increases the required main gear length. Alternatively the angle of attack at landing could be lowered to decrease gear length, whereas this measure would increase landing speed. A further constraint is that the main gear has to be positioned aft of the vehicle C.O.G. to avoid back-tilting after main gear touch down.[5] These considerations finally led to a main gear length of about 5 m. The required angle of attack at landing has been estimated to be 16° including a 2° margin, resulting in a landing speed of 280 km/h. For this configuration the main gear carries 84.6 % of vehicle empty weight, the nose gear 15.4 %. This is a comparatively high load percentage for the nose gear according to Ref. 5, but is being considered as acceptable. The length of the gear bay has been determined by using the 5 m main gear length and adding 1 m to account for a mounting and deployment mechanism. The gear bay width has been estimated in a simplified manner by taking the same bay length to width ratio as found for the Space Shuttle in Ref. 6. This results in a gear box width of 2.5 m. Each gear strut is equipped

with 4 tires, yielding a total of 8 tires for the main gear. The tire diameter has been estimated to 1.16 m,[7] with the tire positions approximately at 50 % of the wing chord in retracted position. The minimum gear box height is 1.34 m, leaving 18 cm construction height for structure and TPS. Fig. 6 shows the main gear box integration into the wing.

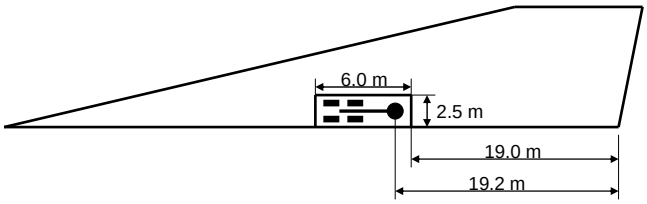

Figure 6. Main gear integration.

2. Flap Sizes and Loads

Preliminary trimming analyses have been conducted to estimate flap sizes for predetermined maximum deflection angles. The discussion of these considerations is not the subject of this paper. However, the resulting flap sizes as well as forces and moments are relevant for wing structure design. The wing is equipped with two flaps of identical sizes. The depth of the flaps including a small actuator adjustment clearance has been estimated to be 3.17 m. For trimming both flaps are planned to be deflected in parallel. However, as a worst case scenario a failure of the inner flap is assumed for the structural analysis, which requires a comparatively high emergency deflection angle for the outer flap to assure vehicle trim. Consequently, the wing is exposed to larger bending moments. The flap structural layout has not been part of the wing structure investigations. Instead, the calculated flap area is simply subtracted from the wing plan form while the flap forces and moments will be introduced as external loads. Fig. 7 shows the initial flap load transmission concept.

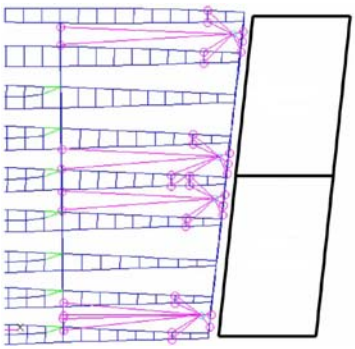

Figure 7. Flap load transmission

3. General Arrangement of Structural Members

The number and position of ribs and spars may have a significant impact on the wing structure mass. Existing large transportation aircraft as well as concepts for hypersonic vehicles have been studied to find useful relationships for rib and spar spacing. Ref. 8 provides a detailed summary for rib and spar spacing for subsonic passenger aircraft. However, these high aspect ratio wings normally use only two or three spars, while the rib spacing is often dictated by fuel sloshing considerations. As an initial assumption a rib spacing of 1.5 m has been used, which according to Ref. 8 is slightly higher than that of the Airbus A380. The ribs are arranged parallel to flow direction, being typical for high speed aircraft. The spar spacing has been fixed to 3 m, which is roughly similar to a hypersonic vehicle concept found in Ref. 9. To maximize structural efficiency the spars are arranged normal to the ribs and parallel to the vehicle main axis. The previously defined spacings are only approximate values, since wing dimensions and gear bay location and size govern the positions of some ribs and spars. The remaining space has been filled in such a manner that the intended spacings will be approximately correct. The result is 9 ribs and 16 spars, including the slant wing box leading and trailing spars. The skin is stiffened by stringers that run in parallel to the spars.

4. Load Cases and Materials

For the initial structural sizing of the wing three different load cases have been taken into account:

- Load case 1: Main gear touch down on a single gear with 1.3 g normal acceleration (empty tanks)
- Load case 2: Subsonic maneuver with 2.5 g normal acceleration and emergency deflection of the outer flap
  - V = 100 m/s, H = 3.0 km, $\alpha = 32°$
- Load case 3: Hypersonic maneuver with 2.5 g normal acceleration and emergency deflection of the outer flap
  - V = 6400 m/s, H = 46.3 km, $\alpha = 12.5°$

The load cases for structural analysis may be adapted in future iterations to account for trajectory changes. The maximum flap loads along the trajectory have been computed for the required deflection angle. For convenience, these values have then been taken for both maneuver load cases. Aluminum has been selected as the structural material for the complete wing. During later investigations also other materials or combinations of different materials may be considered. The material data for the selected aluminum are listed in Table 3. The allowable strength of 360 MPa will be reduced by a safety factor of 1.5, resulting in a final allowable stress of 240 MPa.

Table 3. Material data.

Material	E [MPa]	G [MPa]	ρ [kg/m^3]	σ_{all} [MPa]
Al 2024-T3	73100	27600	2800	360

5. Modelling and Optimisation Approach

PATRAN and NASTRAN have been used for modeling and optimization. All spar/rib webs have been modeled with shell elements, whereas beam elements have been used for the spar and rib caps. The skin model is composed of two layers. The first one is the original skin, while the second one represents a "smeared" stringer layer. The stringer layer has been modeled by an approach derived from Ref. 10 and Ref. 11. The wing has been clamped at the caps of all spars at the wing root. The NASTRAN SOL200 algorithm has been used for structural optimization with the Von Mises stress as the optimization criterion. The load cases 1-3 have been treated successively. The required wall thicknesses of a load case have been set as the lower bound for the next load case. Minimum wall thicknesses have been set to account for manufacturing issues.

The original set up for the wing considered the thickness of each skin panel (the area between two ribs and two spars) individually. The same was true for rib and spar webs and caps. Skin layer and smeared stringer layer have been considered separately. However, the resulting large number of design variables led to very high computation times. Thus, the number of variables had to be reduced. This has been done by defining a fixed relationship between skin and stringer layer thickness. In addition, several skin panels as well as rib and spar section have been merged in larger regions with constant thicknesses. These measures finally yielded 122 design variables. Excessive plate bending and buckling have initially been addressed by manually adapting wall thicknesses in critical regions after the optimization process.

Not the total profile height of the wing can be used for constructing the structure. The TPS may require a non-negligible portion of the profile height. As an initial guess a TPS thickness of 10 cm has been assumed for the lower surface, and 2 cm for the upper surface. The available construction height has been reduced by these values. Further iterations will be done later, incorporating the required thicknesses generated in TPS investigations. This will be discussed in Section IV.

6. Initial Static Optimization Results

Table 4 lists the total structural mass for one wing after optimization for the three load cases and the final manual rework. The mass does not include the flap structure.

Table 4. Wing structure mass evolution.

Load case	Wing structural mass [kg]
1	3564
2	7617
3	8375
Manual adaption	8788

The deformation of the structure for load case 1 is displayed in Fig. 8. The gear load introduction led to thickness adaptions in the gear bay section, while a large part of the wing remained on the predefined minimum thickness value.

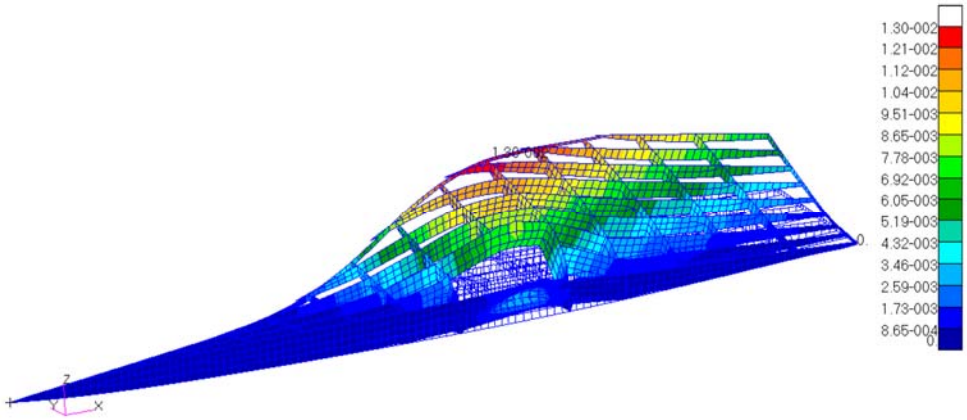

Figure 8. Wing deformation for main gear touch down.

Load case 2 and 3 led to strong structural adaptions in the rear part of the wing, which is a result of the local load transmission of the flaps. The deformation displayed in Fig. 9 clearly describes the effect of the flap load introduction. Fig. 10 and Fig. 11 show the Von Mises stresses for load case 2 for the rib/spar skeleton and the skin. As may be observed in Fig. 11 the stress in the skin exceeds the limitation of 240 MPa. This is a result of the two layer definition of the skin. To overcome this problem the skin in the critical regions has simply been adapted manually.

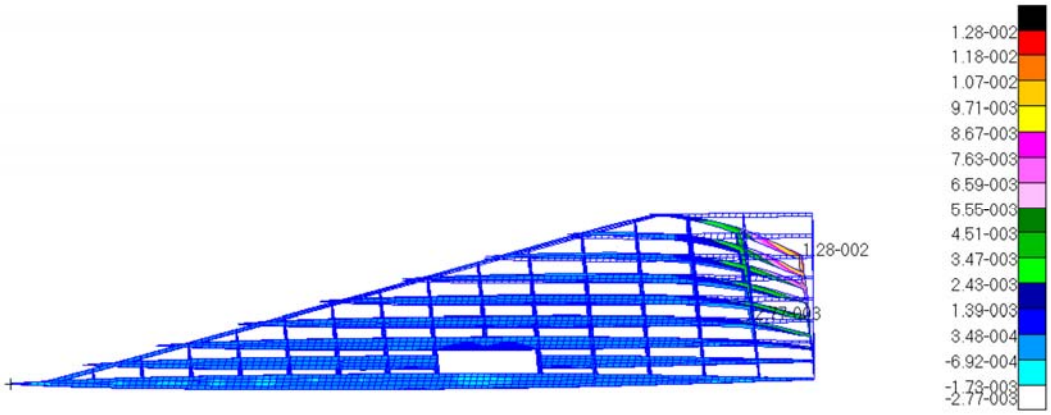

Figure 9. Wing deformation for hypersonic maneuver with flap deflection.

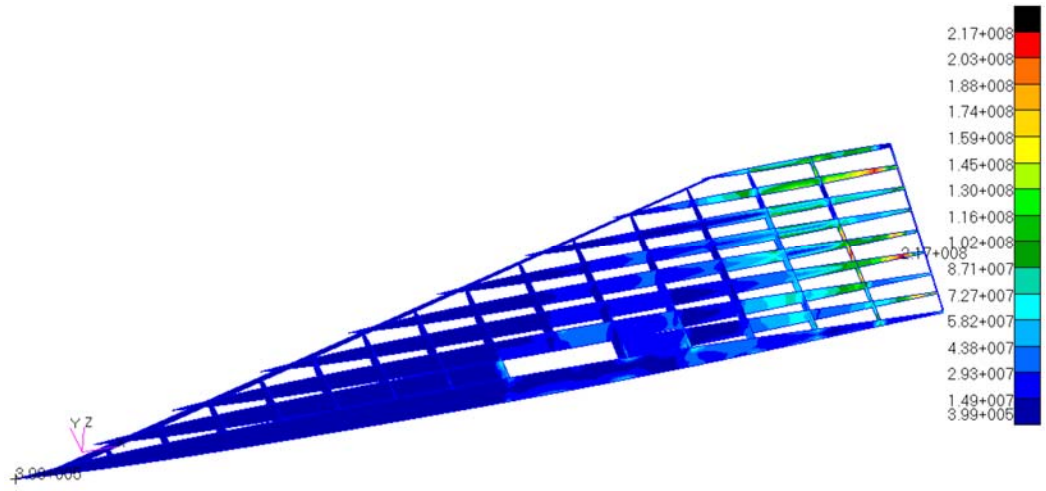

Figure 10. Von Mises stress in ribs and spars for subsonic maneuver with flap deflection.

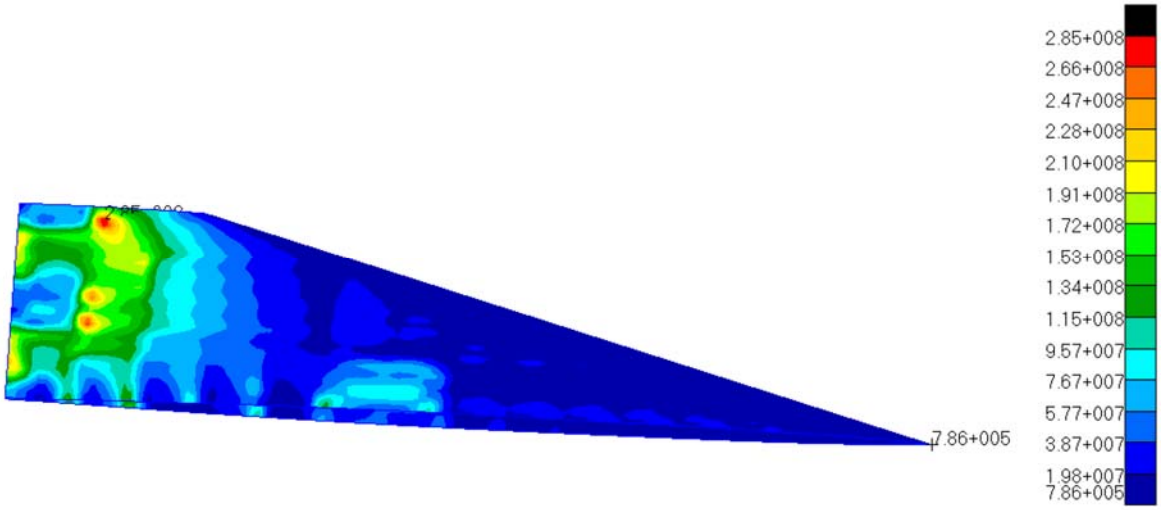

Figure 11. Von Mises stress in wing skin for subsonic maneuver with flap deflection.

It was found that load case 1 and load case 2 already size the majority of the wing, while load case three led only to a comparatively slight mass increase. This is not surprising since the wing in load case 2 and 3 has to bear the same lift and flap forces, while only the lift distribution differs.

The final thicknesses of upper and lower skin, spars and ribs are shown in Fig. 12 to Fig. 15. Note, that the thickness of the skin displayed here is the combined thickness of the "real" skin and the smeared stringer layer. The actual skin thickness is only 12 % of the displayed total thickness, while the remainder is formed by the smeared stringer layer. All thicknesses are given in [m].

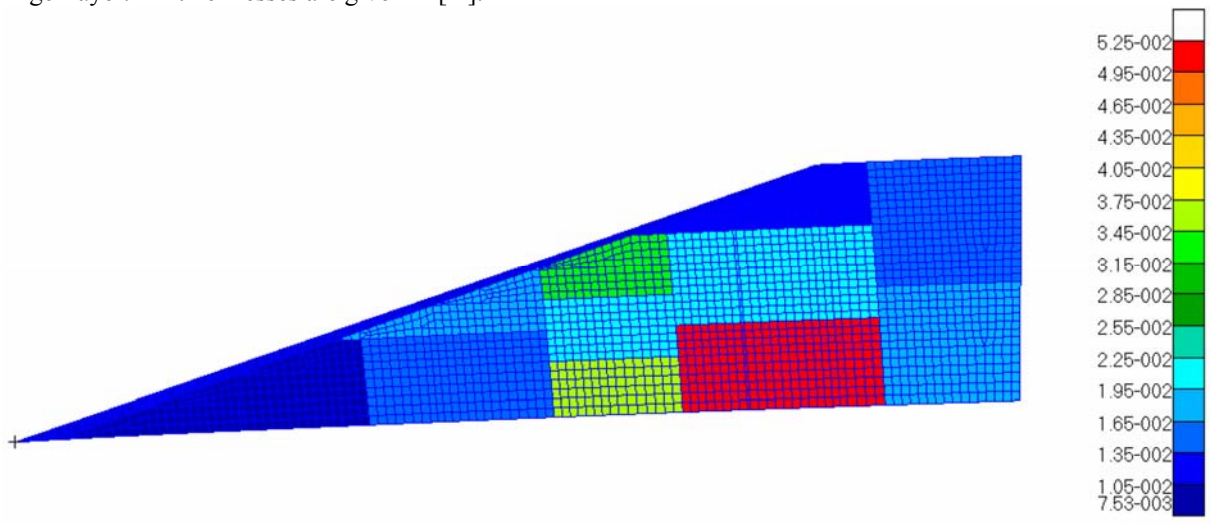

Figure 12. Upper wing skin thickness – skin layer and smeared stringer layer.

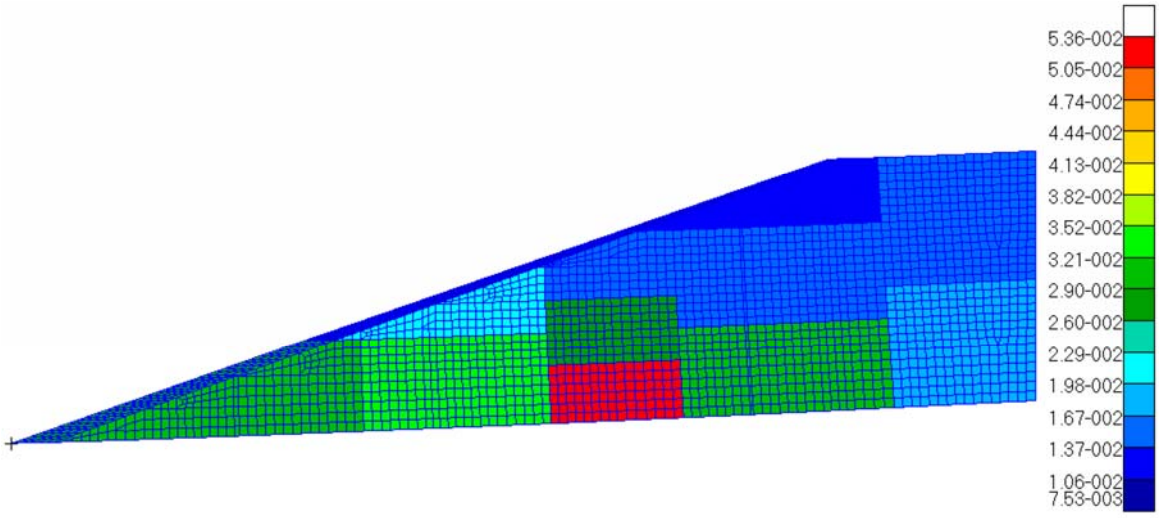

Figure 13. Lower wing skin thickness – skin layer and smeared stringer layer.

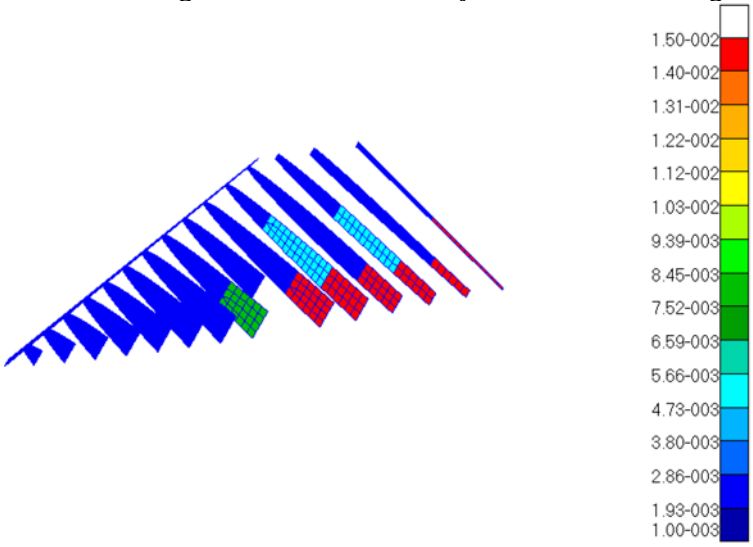

Figure 14. Spar web thicknesses.

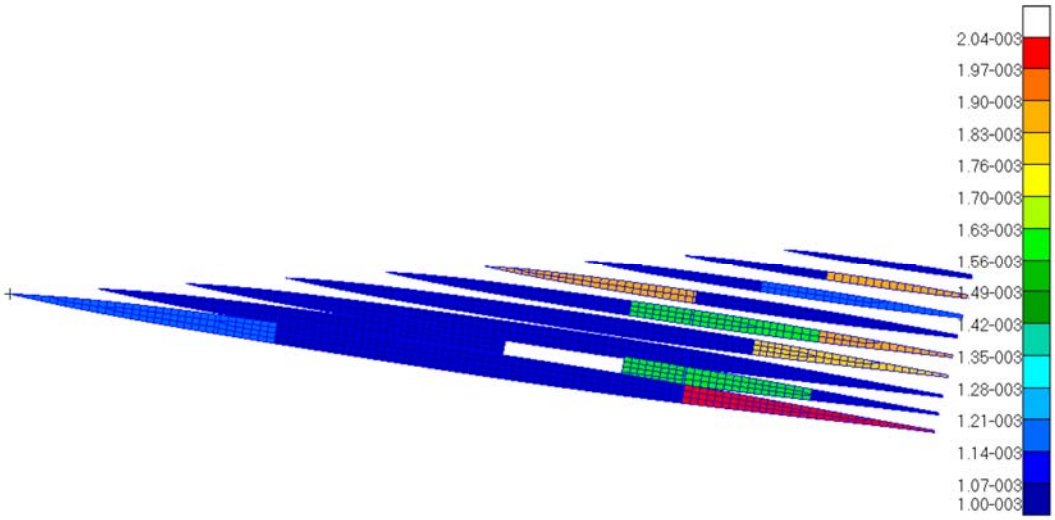

Figure 15. Rib web thicknesses

7. Structural Dynamic Analysis

The web thicknesses in ribs and spars are free parameters determined by the structural optimization of the wing. Examination of the results from an eigenvalue analysis performed after the initial wing structure optimization revealed that local bending modes for the webs were dominating. This lack of local out-of plane stiffness may have an effect also on the global stability of the wing that needs to be taken into account.

After a manual modification of the model some average beam web thicknesses are used over a limited number of larger areas. It is common practice in aircraft design to attach vertical stiffeners to the webs at regular intervals to control buckling of the webs. To obtain a similar effect the thin homogenous aluminium plates in the webs are replaced by aluminium sandwich panels with a low-density core material. The sandwich skins having half the original web thickness keeps the in-plane shear stiffness unaltered, whereas out-of plane stiffness increases. In the calculation, the core material properties, the module of elasticity E, Poisson's ratio ν, and mass density ρ, are set to 500 MPa, 0.3 and 50 kg/m^3 respectively. The thickness of the core material is 1 cm. In Fig. 16, the yellow areas are webs replaced by the sandwich structure. The blue, orange and red areas, in Fig. 16, are unchanged as the estimated thickness of the homogeneous aluminium web is large, due to high loads, resulting in thicknesses comparable with the thicknesses proposed for the sandwich panels.

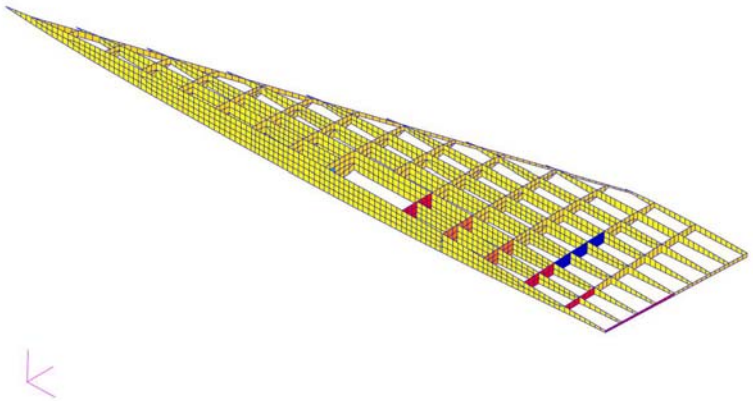

Figure 16. Sandwich reinforcement thickness distribution.

With the model of the wing altered as described above and with the wing displacement constrained along the wing-root, the eigenfrequencies were determined as given in Table 5. The corresponding shapes for the first six modes may be observed in Fig. 17. The result for the modified structure shows that the first two modes are global, with the lowest eigenfrequency estimated at 8.87 Hz. Skin deformation may be observed for modes three and four. Modes three and four are also global in character. Starting from mode five a local skin panel vibration is clearly visible, *e.g.* at the landing gear bay. However, the calculated frequencies for these modes are relatively high, but may be improved by modifying the skin properties.

Table 5. Modal frequencies for the wing.

Mode Number	Mode Frequency (Hz)
1	8.87
2	18.2
3	25.5
4	27.5
5	30.7
6	33.8
7	34.6
8	35.0
9	35.4
10	36.6

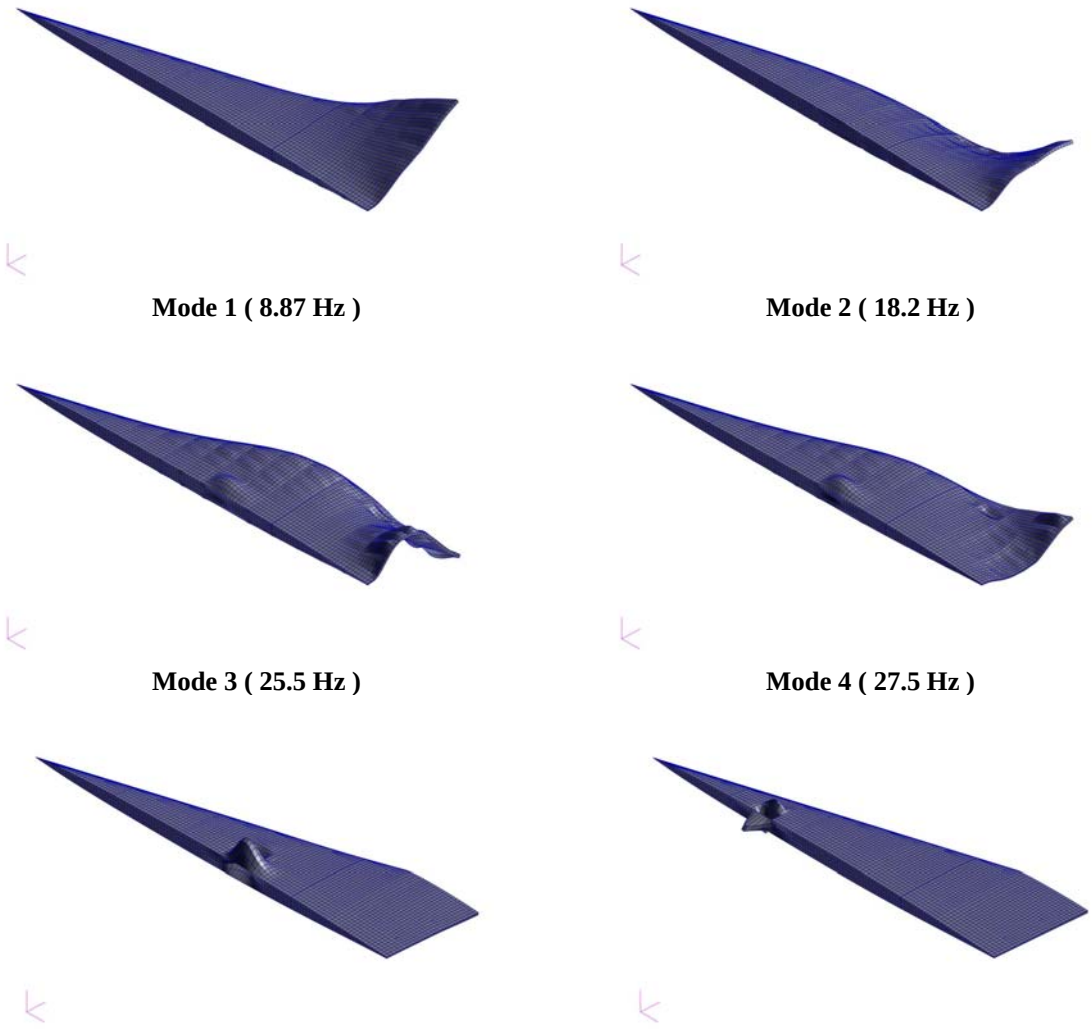

Mode 1 (8.87 Hz) **Mode 2 (18.2 Hz)**

Mode 3 (25.5 Hz) **Mode 4 (27.5 Hz)**

Mode 5 (30.7 Hz) **Mode 6 (33.8 Hz)**

Figure 17. The first six elastic wing mode shapes.

It is concluded that in a future improved structural optimization, a frequency constraint that is based on stability considerations should preferably be added in order to avoid sub-optimization and significant weight penalties. In the following section a conceptual model of the fuselage structure is added in order to introduce a more realistic global boundary condition, than the rigid one used in the investigation so far.

B. Preliminary Fuselage Model and Wing-Fuselage Integration

The wing structure model is assembled with models of the fuselage and the fin into a preliminary conceptual global model of the Orbiter. The wing geometry is blended to fit with the fuselage shape, keeping the leading edge sweep and length, and the overall wing-profile. Fuselage frame pitch was chosen as the distance between the wing-spars (typically 3 m) for this first design iteration. A smaller frame pitch is very likely in a final design. The finite element mesh for the Orbiter is shown in Fig. 18. Mass elements representing everything from fuel to landing-gears are introduced at six nodal points around the perimeter at each frame-station, giving a total of 176 mass-points. Internal structures such as, for instance, the oxygen and hydrogen-tanks are not modelled at present.

The wing is low mounted on the fuselage and the stiffness of the beams being part of the frames in the lower fuselage becomes critical for the rigidity of the wing attachments. As there are liquid oxygen and hydrogen fuel-tanks located in the center and rear part of the fuselage the height of the wing-carry through beams are constrained

in this part of the fuselage. In the first few iterations being described here only the eigenfrequencies and modes are considered. Stress constraints and aeroelasticity will be considered later. To prevent low-frequency vibrations dominated by the deformation of the fuselage cross-sections it was attempted to use only the stiffness of the fuselage frames. The weight-penalty experienced when trying to significantly increase these frequencies is extreme. It is concluded that other means of preserving the cross-section shape, such as a bulkheads or truss-structures, must be introduced. Hence, triangular truss-structures are created from three rods connected to each other at their ends, and being connected at the corners to the fuselage frame. The three connection-points chosen here are the top of the fuselage roof and the upper wing-attachment points at each side. Four of these triangular trusses are introduced. One truss is introduced directly behind the position for the LH-tank, one at each end of the LOX-tank, and the fourth in front of the location for the passenger module. With the introduction of these reinforcements the fifth lowest frequency still contains a significant interaction between fuselage deformation near the middle of the fuselage where the heavy oxygen-fuel is located and the wing- and fin-bending. This mode may be seen in Fig. 19.

The lowest fundamental vibration frequencies are calculated and examined. The first frequency, corresponding to fuselage bending, is 4.2 Hz with filled tanks. Without fuel this frequency increases to 4.9 Hz, and the wing-bending mode is 6.1 Hz. This may be compared to 8.87 Hz for the wing when clamped to a rigid wall. The bending-mode for the configuration without fuel is shown in Fig. 20.

The data given here illustrates the results from the first iterations and obviously many iteration remains with more refined models. Further optimization is expected to increase the frequencies calculated here, but it should be remembered that strength and aeroelastic constraints may require redesign with an influence on eigenfrequencies and an increase in the structural weight.

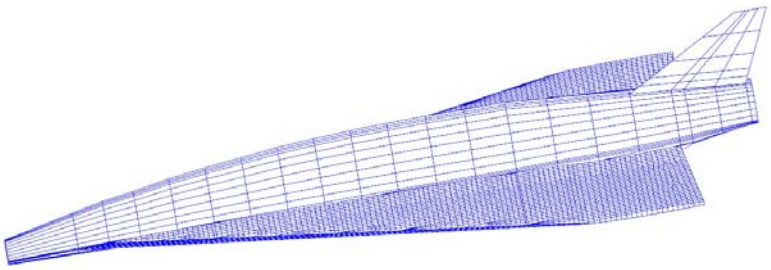

Figure 18. Mesh for preliminary conceptual structural analysis of the orbiter.

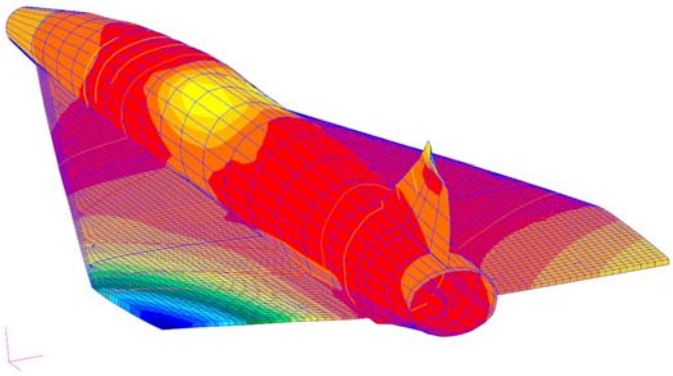

Figure 19. Mode five is influenced by fuselage deformation due to heavy oxygen-fuel in the center fuselage. Frequency 6.1 Hz.

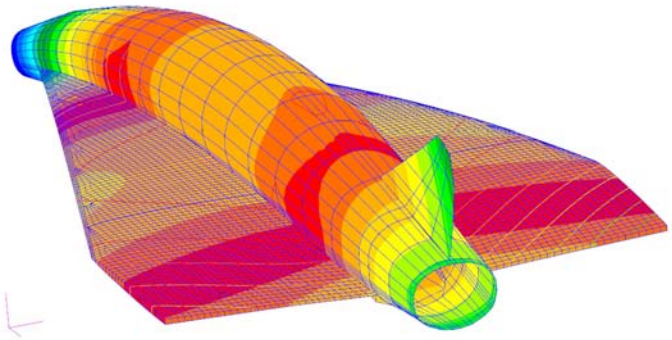

Figure 20. First bending mode for the orbiter with zero fuel load. Frequency 4.9 Hz.

IV. Preliminary Design of Thermal Protection System

During re-entry or gliding flight the passenger stage is exposed to severe aerodynamic heating. Already in an early phase of the SpaceLiner studies it has been decided to follow a TPS protected cold structure approach instead of considering hot structures. Consequently, the total surface of the SpaceLiner passenger stage is TPS protected. The wing and fin leading edges as well as the fuselage nose require active cooling, while the major part of the surface uses passive systems only. A transpiration cooling system has been proposed for the actively cooled regions. This has been investigated by DLR in the past and will soon be the subject of experimental testing.[12] Currently, water is planned to be used as coolant. However, due to possible oxidation problems this might be changed in the future.

A. Thermal Protection System Sizing Methodology

For estimation of the surface temperatures and heat fluxes the DLR code HOTSOSE has been used. This tool combines Modified Newton and Shock Expansion methods. Radiation equilibrium and fully turbulent boundary layers are assumed. Fig. 21 and Fig. 22 show the resulting surface temperatures for the most demanding flight point with Ma = 20.1, H = 59.4 km and $\alpha = 8°$.

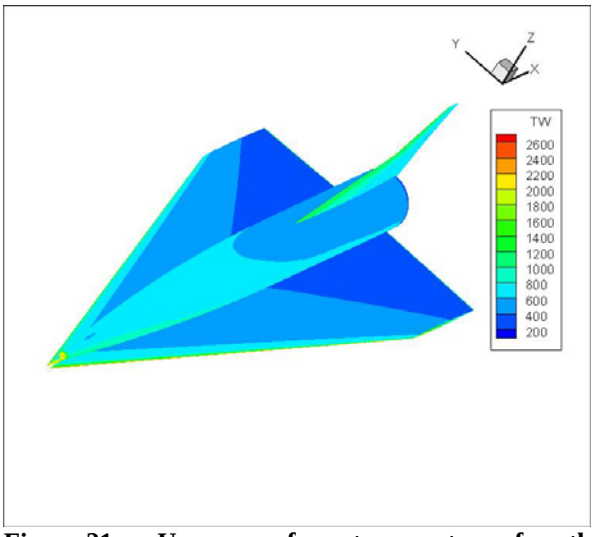

Figure 21. Upper surface temperature for the passenger stage at Ma = 20.1, H = 59.4 km, $\alpha = 8°$.

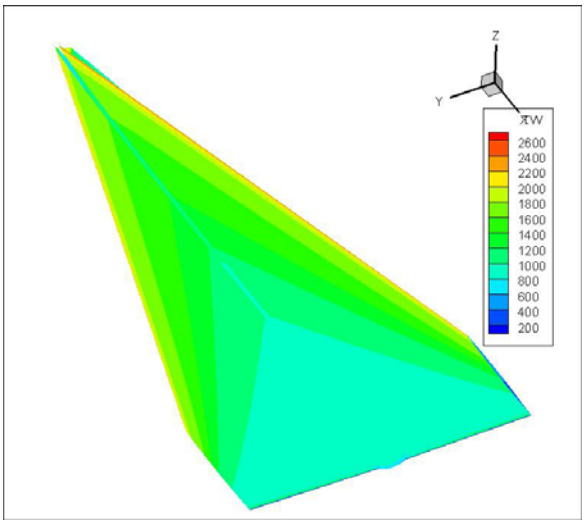

Figure 22. Lower surface temperature for the passenger stage at Ma = 20.1, H = 59.4 km, $\alpha = 8°$.

Heat fluxes and surface temperatures have been computed along the complete trajectory for a number of representative surface points. From these data the maximum heat fluxes and surface temperatures during flight have

been determined for each treated surface point. Finally, the required TPS thicknesses are estimated for each point using a 1-dimensional sizing code. Several TPS materials are being considered, with the lightest one for a given temperature being selected. The TPS thicknesses and corresponding masses that have been found for the representative surface points will be assigned to surfaces with similar heat loads and temperatures. By doing this for the whole vehicle surface, the total TPS mass can be found.

The TPS thicknesses depend heavily on the allowed temperature of the back-structure. As stated previously, the initial structural design utilizes aluminum. The allowed back-structure temperature has been assumed as 400 K. However, this material choice has not been fixed. Other structure materials such as titanium and PEEK may be utilized, too. Thus, two additional investigations have been performed for back-structure temperatures of 530 K and 600 K. The following sub-sections describe the TPS materials considered in this investigation. For each material the insulation thicknesses will be varied, while the thicknesses of the cover panels (if applicable) remain constant.

1. Ceramic Matrix Composite (CMC)

For the high temperature zones ceramic matrix composite (CMC) has been selected. The TPS setup has been derived from the REX Free Flyer studies performed by DLR. The TPS consists of a 6 mm strong CMC cover panel which is attached to the back structure with flexible insulation in between. The CMC panel thickness has been directly taken from the REX studies and will be held constant. The insulation material instead has been changed from the original combination of ZIRCAR Sali, EADS HTI and EADS IFI to ZIRCAR alumina mat. The maximum allowed temperature for the alumina insulation has been fixed to 1923 K. For the actively cooled regions this material has been selected, too.

2. Conformable Reusable Insulation (CRI)

For protection of the areas with intermediate temperatures Boeing's Conformable Reusable Insulation (CRI) was selected, which has been used on the X-37 re-entry vehicle.[13] According to Ref. 14 CRI is made of a metal Inconel 617 fabric, a ceramic NEXTEL fabric and flexible alumina insulation in between. The same ZIRCAR alumina mat is assumed as for the CMC based TPS described previously. The maximum allowed surface temperature is limited by the maximum allowed temperature of the Inconel cover layer, which is assumed here to be 1373 K according to data from Ref. 15. CRI is waterproof and has a comparatively low surface roughness.

3. Advanced Flexible Reusable Insulation (AFRSI)

AFRSI will be applied for low to intermediate temperature regions. The material has already been in use on the leeward side of the Space Shuttle. According to Ref. 16 it has a maximum multi-use temperature of 922 K.

4. Felt Reusable Surface Insulation (FRSI)

Felt Reusable Surface Insulation (FRSI) consists of a NOMEX blanket which is coated with a silicon elastomer. The coating is used to waterproof the felt. FRSI is very lightweight and can be used up to temperatures of 672 K. It will be used for surfaces exposed to lower temperatures.

The four TPS materials mentioned previously are combined to cover the whole vehicle surface and form the initial baseline TPS concept.

In theory it would be the most mass efficient solution to optimize the TPS thickness for every point of the vehicle surface. However, this is not only unpractical for this preliminary study, but would also bear logistical challenges for TPS manufacturing and maintenance of a real vehicle. Instead, several thickness layers have been defined here for each type of material. For CRI three thickness layers have been defined and two for each of the other materials. Table 6 lists all thickness layers and their corresponding area specific masses. For each back-structure temperature T_b individual thickness layers have been defined.

Table 6. TPS thickness layers for different back-structure temperatures.

Material	Maximum temperature [K]	T_b = 400 K		T_b = 530 K		T_b = 600 K	
		Thickness [cm]	Area specific mass [kg/m^2]	Thickness [cm]	Area specific mass [kg/m^2]	Thickness [cm]	Area specific mass [kg/m^2]
CMC-Alumina water cooled	2000	25.74	20.2	17.5930	17.3475	14.3068	16.197
CMC-Alumina-1	2000	22.947	19.228	13.8306	16.0307	10.9318	15.0155
CMC-Alumina-2		20.975	18.521	11.4577	15.2002	8.8300	14.2805
CRI-1	1373	17.577	9.2127	8.4846	6.0342	6.2899	5.2661
CRI-2		14.973	8.305	6.7037	5.4109	4.3873	4.719
CRI-3		12.954	7.599	5.4556	4.9741	3.6991	4.3593
AFRSI-1	922	4.802	6.413	1.7073	2.4463	1.3249	1.9563
AFRSI-2		3.888	5.241	1.3350	1.96914	0.6872	1.1391
FRSI-1	672	2.280	3.1802	0.120	1.0131	0.120	1.0131
FRSI-2		2.204	2.1735	0.020	0.300	0.020	0.300

B. Results

Table 7 breaks down the total TPS masses in the individual TPS materials and Fig. 23 and Fig. 24 show the material distribution across the surface for the 400 K back-structure temperature case. As may be observed the CMC-Alumina has the highest mass fraction of all materials. Large parts of the lower wing surface are covered by CMC. FRSI instead has a very low mass fraction, although it covers the total upper wing surface and parts of the upper fuselage. Not surprising, the lower wing surface requires the major part of the TPS mass with more than 2/3 of the total mass.

Table 7. TPS mass breakdown for different back-structure temperatures.

Material	Mass [kg] (T_b = 400 K)	Mass [kg] (T_b = 530 K)	Mass [kg] (T_b = 600 K)
CMC-Alumina water cooled	1801.11	1546.77	1444.19
CMC-Alumina-1	6363.06	5304.98	4969.03
CMC-Alumina-2	2468.60	2025.98	1903.40
CRI-1	4588.77	3005.59	2623.00
CRI-2	566.923	369.36	322.13
CRI-3	1368.77	895.96	785.22
AFRSI-1	2009.50	766.54	613.00
AFRSI-2	2730.17	1025.76	593.39
FRSI-1	560.06	178.42	178.42
FRSI-2	508.73	70.22	70.22
Water	7245.49	7245.49	7245.49
Total	30211.2	22435.1	20747.5

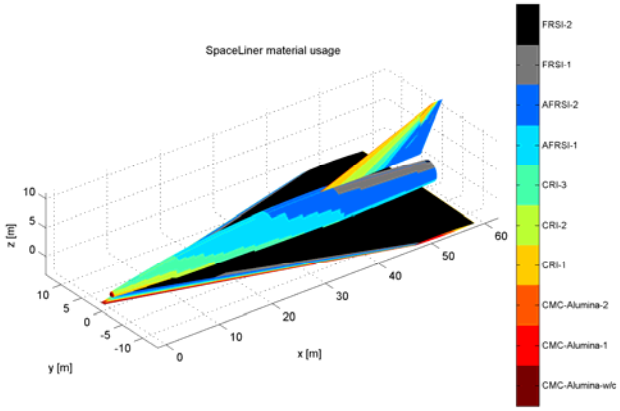

Figure 23. Upper surface TPS material distribution.

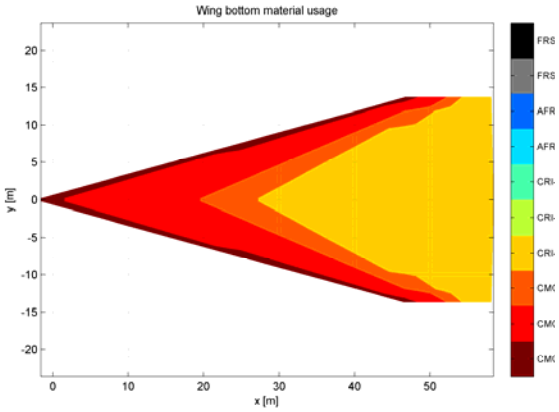

Figure 24. Lower surface TPS material distribution.

C. Impact on Structural Design

During the TPS investigations it has been found that the required FRSI thicknesses on the upper side of the vehicle match fairly well the 2 cm originally anticipated in the wing structure analysis. However, the thicknesses on the lower side of the vehicle are higher than assumed. Further iterations will consider the computed TPS thicknesses and the wings structure construction height may be adapted. Due to lower geometrical moments of inertia this might slightly increase wing structure mass. Alternatively, a thicker wing profile could be selected, having an impact on the hypersonic flight characteristics. A corresponding trade off will be done to identify the most advantageous solution.

V. Conclusion

In the present paper the current status of the preliminary structural and thermal protection system layout for the SpaceLiner passenger stage has been described. Potential load cases have been identified and presented. The wing structure design has been discussed in detail, while for the fuselage only rough analyses have been done so far. A TPS concept has been defined and described for the complete vehicle The previous activities have shown the importance of considering design details such as TPS, gear or flap integration already in the early phases of the structural layout. In future works the wing design will be further optimized and the TPS will be integrated into the structural design process. Special attention will be paid to the design of the fuselage primary structure and the integration of wings, propellant tanks and the rescue stage.

Acknowledgments

Part of this work was performed within the 'Future High-Altitude High-Speed Transport 20XX' project investigating high-speed transport. FAST20XX, coordinated by ESA-ESTEC, and supported by the EU within the 7th Framework Programme Theme7 Transport, Contract no.: ACP8-GA-2009-233816.
Further information on FAST20XX can be found on http://www.esa.int/fast20xx.

The authors gratefully acknowledge the contributions of Ms. Carola Bauer, Ms. Ingrid Dietlein, Mr. Björn Nagel, Mr. Paul Nizenkov and Mr. Tobias Schwanekamp. Special acknowledgments belong to Mr. Bryan Tong Minh and Mr. Daniel Keller, whose work has been essential for this paper.

References

[1]Sippel, M.: "SpaceLiner – a Visionary concept of an Ultra Fast Passenger Transport under Investigation in FAST20XX", AIAA-2009-7439, *16th International Space Planes and Hypersonic Systems and Technologies Conference*, Bremen, Germany, 2009

[2]Van Foreest, A.: "The Progress on the SpaceLiner Design in the Frame of the FAST20XX Program", AIAA-2009-7438, *16th International Space Planes and Hypersonic Systems and Technologies Conference*, Bremen, Germany, 2009

[3]Sippel, M., Van Foreest, A., Dietlein, I., Cremaschi, F.: "System Investigations of the SpaceLiner Concept in FAST20XX", *17th International Space Planes and Hypersonic Systems and Technologies Conference*, San Francisco, 2011 (submitted for publication)

[4]European Aviation Safety Agency, "Certification Specifications for Large Aeroplanes CS-25", Amendment 2, October 2006

[5]Roskam, J.: "Airplane Design Part II: Preliminary Configuration Design and Integration of the Propulsion System", Roskam Aviation and Engineering Corporation, Ottawa, Kansas, 1989, chapter 9

[6]Gong, L., Ko, W. L., Quinn, D.: "Thermal Response of Space Shuttle Wing During Reentry Heating", NASA TM-85907, 1984

[7]Roskam, J.: "Airplane Design Part IV: Layout Design of Landing Gear and Systems", Roskam Aviation and Engineering Corporation, Ottawa, Kansas, 1989, chapter 2

[8]Sensmeier, M. D., Samareh, J. S.: "A Study of Structural Layouts in Post-WWII Aircraft", *45th AIAA/ASME/ASCE/AHS/ASC Structures, Structural Dynamics and Materials Conference*, Palm Springs, California, April 2004

[9]Bardenhagen, A.: "Massenabschätzung und Gesamtauslegung der Unterstufe von Hyperschall-Raumtransportern", Ph. D. Dissertation, Institute of Aircraft Design and Lightweight Structures, Technical University of Braunschweig, 1998

[10]Ciampa, P. D., Nagel, B., Van Tooren, M.: "Global Local Structural Optimization of Transportation Aircraft Wings", 51st AIAA/ASME/ASCE/AHS/ASC Structures, Structural Dynamics, and Materials Conference, Orlando, Florida, April 2010

[11]Ciampa, P. D.: "Global-Local Optimization of Stringer Stiffened Panels for Transportation Aircraft Wings", MSc Thesis, Faculty of Aerospace Engineering, Delft University of Technology, 2009

[12]Van Foreest, A., Sippel, M., Gülhan, A., Esser, B., Ambrosius, B. A. C., Sudmeijer, K.: "Transpiration Cooling Using Liquid Water", *Journal of Thermophysics and Heat Transfer*, Vol. 23, No. 4, October-December 2009

[13]Scotti, S. J., Clay, C., Rezin, M.: "Structures and Materials Technologies for Extreme Environments applied to Reusable Launch Vehicles", *AIAA/ICAS International Symposium and Exposition* , July 2003, Dayton, USA

[14]Rasky, D., Kourtides, D. A., Dittman, D. L., Rezin, M. D., Hiel, C., Vallotton, W. C.: "Durable Advanced Flexible Reusable Surface Insulation", United States Patent number 5811168, September 22th, 1998

[15]ThyssenKrupp VDM, Nifcrofer 5520 Co-alloy 617 material data sheet no. 4019, January 2005

[16]Rezin, M., Oka, K.: "The Evolution of Flexible Insulation as Thermal Protection Systems for Reusable Launch Vehicles: AFRSI (Advanced Flexible Reusable Surface Insulation) to CRI (Conformal Reusable Insulation)", *National Space and Missile Materials Symposium*, June 2001